ACS OMEGA

http://pubs.acs.org/journal/acsodf

Article

An Insight into the Effects of SnF_2 Assisting the Performance of Lead-Free Perovskite of $FASnI_3$: A First-Principles Calculations

Wei Xie, Liping Peng, and Neng Li*

Cite This: *ACS Omega* 2021, 6, 14938−14951

Read Online

ACCESS | Metrics & More | Article Recommendations | Supporting Information

ABSTRACT: It is an effective method to use SnF_2 and SnF_4 molecules to assist in enhancing the performance of $FASnI_3$ perovskite. However, the mechanism in this case is not clear as it lacks a certain explanation to specify the phenomenon. Through first-principles calculations, this paper constructed several modes of SnF_2 and SnF_4 adsorbed on the surfaces of $FASnI_3$ and explored adsorption energies, band structures, photoelectric properties, absorption spectra, and dielectric functions. The SnF_2 molecule adsorbed at the I5 position on the FAI-T surface has the lowest adsorption energy for the F atom, which is 0.5376 eV. The Sn−I bond and Sn−F bond mainly affect the photoelectric properties of $FASnI_3$ perovskite solar cells, and the SnF_2 adsorption on the FAI-T surface can effectively strengthen the bond energies, which shortens the bond lengths of the Sn−I and Sn−F bond, and eliminate surface unsaturated bonds to passivate the surface defects. Furthermore, the probability of energy transfer was lower between the SnF_2 molecule and the ion around it than between SnF_4 and its ion. Especially, in the aspect of optical properties, we found that the intensity of the absorption peak of SnF_2 adsorption increase was larger than that of SnF_4 adsorption. Additionally, the static dielectric constants of SnF_4 adsorption on the two surfaces, denoted SnF_4, made the perovskite respond more slowly to the external electric field. Based on this work, we found that SnF_2 had a greater positive effect on the optical property of perovskite than SnF_4. We consider that our results can help to deeply understand the essence of SnF_2 assistance in the performance of $FASnI_3$ and help researchers strive for lead-free perovskite solar cells.

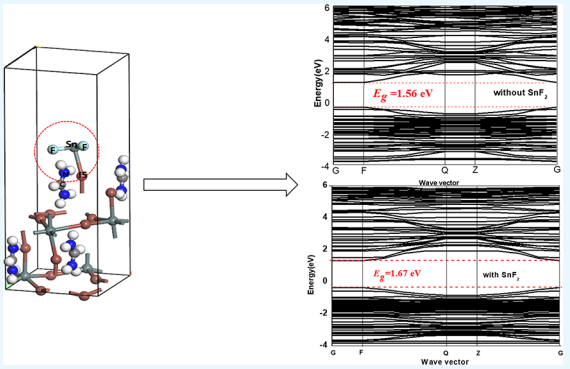

1. INTRODUCTION

Over the past decade, the power conversion efficiencies (PCEs) of organic−inorganic metal halide perovskite solar cells (PSCs) have reached 25.2%, making them promising in commercial applications.[1−14] Lead-based PSCs possess a number of merits, such as a high absorption coefficient, long carrier diffusion distance, low exciton binding energy, and so on. Simultaneously, this kind of material faces huge challenges of environmental protection and atmosphere stability.[15] Hence, it is a common approach to substitute tin for lead in perovskite. Recently, many lead-free perovskite materials have appeared, for instance, $CsSnI_3$, $MASnI_3$, $FASnI_3$, $MAGeI_3$, etc. Compared with lead-based perovskites, tin-based perovskite has the advantage of good absorption. However, its instability and low efficiency impede the performance of its devices.

To optimize the performance of the tin-based PSCs, Lewis base additives are being used, which is effective. Some literature studies reported that by adding a SnF_2 additive to the precursors of $CsSnI_3$, the PCE increased from 3.38 to 3.4%, the open circuit voltage (V_{oc}) increased from 0.40 to 0.41 V, and the short circuit current (J_{sc}) was maintained at 18.0 mA/cm^2.[16] The highest PCE of pure $MASnI_3$ was 6.4%, with a V_{oc} of 0.88 V, J_{sc} of 16.8 mA/cm^2, FF of 42%, and band gap of 1.23 eV.[17] However, when the MA cation (=CH_3NH_3) was replaced by an FA cation (=CH $(NH_2)_2$), the band gap broadened to 1.41 eV[18] at low temperature. $FASnI_3$ can keep a stable structure and has a larger resistivity and lower mobility than $MASnI_3$, indicating that it possesses a lower density of vacancy states.[19] Therefore, $FASnI_3$ possesses a higher stability with a favorable PCE than $MASnI_3$. For instance, Ning and his coworkers prepared a low-dimensional tin-based perovskite with PEA doping, and this kind of perovskite reached a PCE of 5.94% after 100 h in a glovebox.[20] Ke and his team made the PCE of $FASnI_3$ reach 7.14% through doping 10% ethylenediammonium (en), and the PCE was sustained at 6.37% after 1000 h.[21]

In addition, with the purpose of achieving high PCE and long-term stability of perovskite, different sorts of measures were taken. For instance, it is an effective method to take advantage of SnF_2 and its complex for an advanced $FASnI_3$

Received: February 10, 2021
Accepted: May 10, 2021
Published: June 3, 2021

Table 1. Parameters of the Optimized Bulk and Two Surfaces with Different Terminals

bulk surface	final enthalpy (eV)	E_g (eV)	formula	number atoms	a (Å)	b (Å)	c (Å)
bulk $FASnI_3$	−7261.040	0.868	$C_4H_{20}N_8Sn_4I_{12}$	48	8.818	12.416	8.857
(010) surface with SnI_2-T	−7261.462	1.205	$C_4H_{20}N_8Sn_4I_{12}$	48	8.857	8.8175	21.492
(010) surface with FAI-T	−7260.836	1.157	$C_4H_{20}N_8Sn_4I_{12}$	48	8.818	23.842	8.857

film. Zong et al. pointed out that SnF_2 remained in grain boundaries of polycrystalline films when they put SnF_2·3FACl into the precursors of $(FAPbI_3)_{0.7}(CsSnI_3)_{0.3}$.[22] In the conditions of high humidity or strong light exposure, the structural phase was stable with or without utilizing any additive. They claimed that SnF_2 played a significant role in the device. Coincidentally, Lee et al. demonstrated that the PCE of $FASnI_3$ reached 4.8% with 10 mol SnF_2−pyrazine doping,[23] and then in darkness and in atmosphere conditions, the PCE was retained at 98% of the initial value. In their work, they declared that pyrazine played a vital role in optimizing the surface morphology, making it smoother and denser. Plenty of work showed that the Sn^{2+} cation promoted the performance of the $FASnI_3$ film.[24−26] However, they lack any theoretical proof to clarify the working mechanism of SnF_2. It is important to explain why the SnF_2 additive enhances the stability of $FASnI_3$.

In this article, the first-principles method was utilized to analyze the interaction between fluorides and perovskite surfaces. Four types of models were built, and their electronic, structural, and optical properties were analyzed. Based on these results, the inner mechanism of SnF_2 bettering the performance of $FASnI_3$ was understood.

2. CALCULATION SECTION

2.1. Parameter Setting. Based on the first principle, the CASTEP[27] model was chosen. After geometric optimization procedure, our calculations are performed by employing density functional theory with the plane wave projector augmented wave method (PAW) as implemented in the Vienna ab initio package.[28] The exchange correlation is approximated by the GGAs PBE[29] and PBEsol[30] and the hybrid functional HSE06 where the Hartree−Fock screening parameter μ is set at 0.2 $Å^{-1}$. HSE06 usually gives band gaps closer to experimental values than GGA results and is useful for calculating the dielectric function despite the fact that it is computationally very expensive. Structural optimization can be performed efficiently with GGAs, and therefore the structural optimization in this study is done employing the GGAs only. To obtain the equilibrium structural parameters, the volume and the ion positions of the crystal are fully relaxed using the PBE and PBEsol approximations. Stability studies were performed by comparing the cohesive energy of the chalcopyrite phase relative to five other potential structural phases of the lattice parameters of orthorhombic $FASnI_3$ where a = 8.8175 Å, b = 12.416 Å, and c = 8.867 Å.[31] The cutoff energy of the plane wave was 380 eV. Either in geometric optimization or in electronic property calculation, the K point[32] in the Brillouin zone[33] was 3 × 3 × 2. The energy band gap of the 2 × 2 × 2 supercell of $FASnI_3$ optimized was 0.868 eV, corresponding to the experimental result.[34] As for the surface, the vacuum thickness was 10 Å. The self-consistent field (SCF) energy tolerance convergence was 5×10^{-6} eV/atom. The max force, max stress, and max displacement were 0.02 GPa, 0.01 eV/atom, and 5×10^{-4} eV/atom, respectively. The detailed experimental structural information of $FASnI_3$ can be learned somewhere else.[35−38] For $FASnI_3$, the electronic configuration was $1s^1$ for H, $2s^22p^2$ for C, $2s^22p^3$ for N, $5s^25p^2$ for Sn, $5s^25p^5$ for I, and $2s^22p^5$ for F.

2.2. Adsorption Energy Calculation. The formula of the adsorption energy is as follows:[39]

$$E_{ads} = E_{molecule/surf} - (E_{molecule} + E_{surf}) \quad (1)$$

in the formula above (1), E_{ads}, $E_{molecule/surf}$, $E_{molecule}$, and E_{surf} stand for the adsorption energy of the system, the total energy of the system, the total energy of a molecule adsorbed, and the total energy of the clean surface, respectively. The lower the adsorption energy, the more stable the surface.

2.3. Effective Mass Calculation. The calculation formula of the effective mass is as follows:[40]

$$m^* = \hbar^2 / \left(\partial^2 \varepsilon(k) \Big/ \partial k^2\right) \quad (2)$$

In the formula mentioned above, m^* represents the electron or hole effective mass, $\hbar$ represents the reduced Planck constant, and $\varepsilon(k)$ represents the energy level of wavevector k. Generally, according to the particle curve of the maximum of the valence band and the curve of the minimum of the conduction band, it is convenient to calculate the electron or hole effective mass.

2.4. Optical Properties and Dielectric Function. The relationship between absorption coefficient and dielectric function is as follows:[41]

$$\alpha = (\sqrt{2})\omega[\sqrt{\varepsilon_1(\omega)^2 + \varepsilon_2(\omega)^2} - \varepsilon_1(\omega)]^{1/2} \quad (3)$$

in the formula above, α, ω, ε_1, and ε_2 represent the absorption coefficient, the frequency, the real part of the dielectric function, and the imaginary part of the dielectric function, respectively.

The complex dielectric function formula is as follows:

$$\varepsilon = \varepsilon_1(\omega) + i\varepsilon_2(\omega) \quad (4)$$

The dielectric function ε is referred to as the complex dielectric function with the real part ε_1 and the imaginary part ε_2. ε_1 symbolizes the polarization intensity of the medium under the condition of an external electric field, which is the ability to bind to a charge. ε_1 at low frequency (=0) stands for the static dielectric constant, reflecting the dielectric response of the material to a static electric field. ε_2 is caused by the relaxation polarization induced by the fact that the various steering polarizations in the material cannot keep up with the change of the external high frequency electric field, which represents the loss of the material under lighting. Light absorption of the interband transition occurs when radiated electrons are perturbed by the electromagnetic field, jumping from the low occupied state to the high unoccupied state.

3. RESULTS AND DISCUSSION

3.1. Stable Geometric Configuration of Surface Adsorption. Before studying the performance after SnF_2 and SnF_4 molecule adsorption, it is essential to select a surface

https://doi.org/10.1021/acsomega.1c00767
ACS Omega 2021, 6, 14938−14951

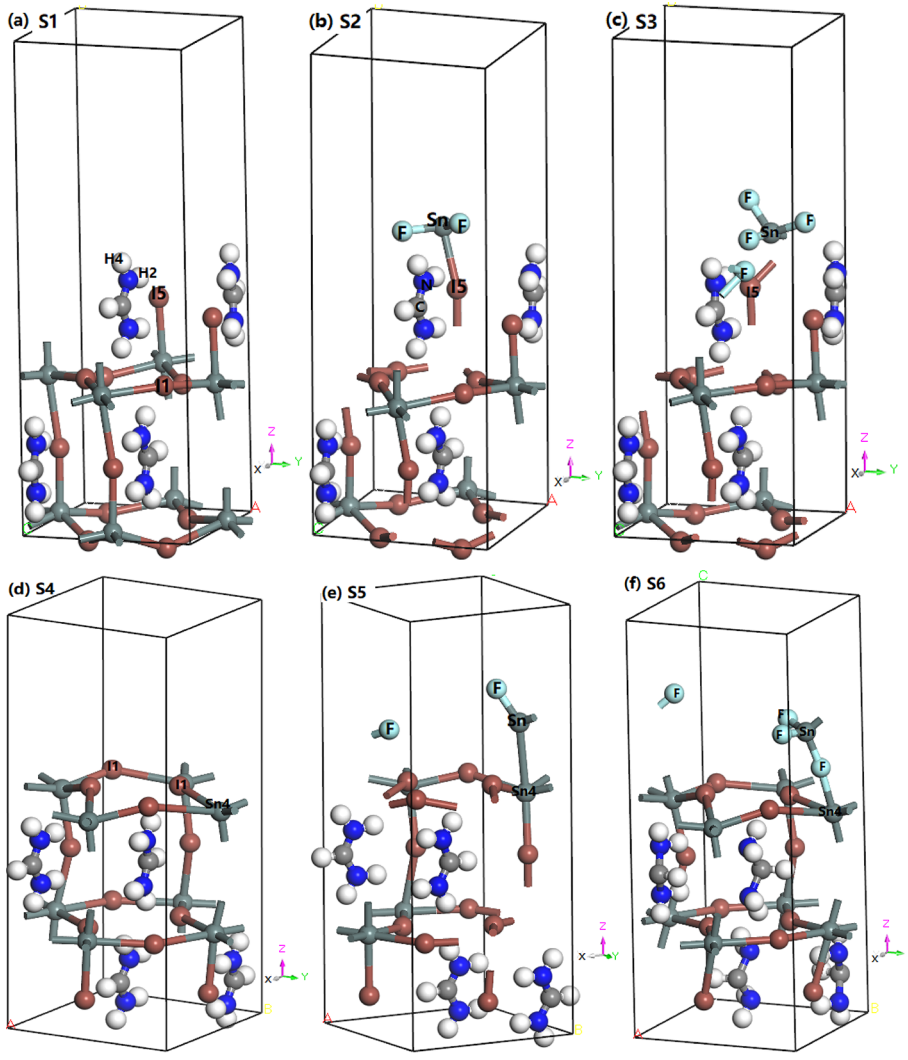

Figure 1. Model structures: of (a) S1, clean FAI-T surface; (b) S2, $Sn(SnF_2)$@I5@FAI-T; (c) $F(SnF_4)$@I5@FAI-T; (d) clean SnI_2-T; (e) $Sn(SnF_2)$@Sn4@SnI_2-T; and (f) $F(SnF_4)$@Sn4@SnI_2-T.

with high stability as the adsorption surface. We picked out two surfaces, FAI-terminal (FAI-T) and SnI_2-terminal (SnI_2-T). When the proportions of SnI_2 and FAI are not equal, there exist two surfaces, the SnI_2-T and FAI-T surface. If the surface is rich in FAI precursors, it forms an FAI-T surface. Similarly, if it is rich in SnI_2, it forms a SnI_2-T surface, and on it, the (100) low index surfaces were selected. As all the thicknesses of the surface slabs were the same and their supercell units were 2 × 2 × 2, the atom numbers of the bulk structure were similar to that of the two surfaces. When these models were optimized, several parameters are gathered in Table 1. For the FAI-T surface, four adsorption locations, considering the SnF_2 or SnF_4 adsorption, contain I5, N1, H4, and H2 atoms. Meanwhile, for SnI_2-T, there are two adsorption locations, including I1 and Sn4, as depicted in Figure 1. For SnF_2 molecule adsorption on the FAI-T surface, there exists eight cases below in total: (1) the Sn atom of the SnF_2 molecule adsorbed at the I5 atom of the FAI-T surface, denoted as $Sn(SnF_2)$@I5@FAI-T; (2) the Sn atom of the SnF_2 molecule adsorbed at the N1 position of FAI-T, denoted as $Sn(SnF_2)$@N1@FAI-T; and (3) the Sn atom of the SnF_2 molecule adsorbed at the H4 atom of the FAI-T surface, denoted as $Sn(SnF_2)$@H4 @FAI-T. The rest can be done in the same manner: (4) the F atom of the SnF_2 molecule adsorbed at the H2 atom of the FAI-T surface, denoted as $Sn(SnF_2)$@H2@ FAI-T. Similarly, there are four cases of F atoms of SnF_2 adsorbing on the FAI-T surface: (5) $F(SnF_2)$@I5@FAI-T, (6) $F(SnF_2)$@N1@FAI-T, (7) $F(SnF_2)$@H4@FAI-T, and (8) $F(SnF_2)$@H2@ FAI-T.

Additionally, we found that SnF_2 oxidized into SnF_4 when it was exposed to air, and we calculated these cases of SnF_4 adsorption on the FAI-T surface, giving eight cases for FAI-T: (1) $Sn(SnF_4)$@I5@FAI-T, (2) $Sn(SnF_4)$@N1@FAI-T, (3) $Sn(SnF_4)$@H4@FAI-T, (4) $Sn(SnF_4)$@H2@FAI-T, (5) $F(SnF_4)$ @I5@FAI-T, (6) $F(SnF_4)$@N1@FAI-T, (7) $F(SnF_4)$ @H4@FAI-T, and (8) $F(SnF_4)$@H2@FAI-T.

Each denotation has its own meaning as mentioned about the FAI-T surface. However, there are a few cases that is not convergent in the calculation process for SnF_2 molecule adsorption on the FAI-T surface, which include (3) $Sn(SnF_2)$ @H4@FAI-T, (4) $Sn(SnF_2)$@H2@FAI-T, (5) $F(SnF_2)$@I5@ FAI-T, and (6) $F(SnF_2)$@N1@FAI-T. For (3) and (4), the two cases failed because tin (Sn) atoms belong to group IA along with hydrogen atoms, losing electrons easily, leading to the mutual repulsion between Sn and H atoms. Thus, the Sn−H bond hardly formed. As for (5), fluorine (F) atoms belong

https://doi.org/10.1021/acsomega.1c00767
ACS Omega 2021, 6, 14938−14951

Table 2. Total Energies and Adsorption Energies of Clean Surfaces and Cases of SnF_2 Adsorption and SnF_4 Adsorption

Terminal	Clean surface or molecule/surf model		Total energy/eV	Eads/eV
FAI-T	Clean (010) surface with FAI-T		-7260.836	--
	SnF_2 @ clean (010) surface with FAI-T	$F(SnF_2)$ @H4	-8681.303	1.201
		$F(SnF_2)$ @H2	-8681.236	1.267
		$Sn(SnF_2)$@N1	-8681.358	1.1452
		$Sn(SnF_2)$@I5	-8681.965	0.539
	SnF_4 @ (010) surface with FAI-T	$Sn(SnF_4)$ @I5	-10006.863	-1.940
		$Sn(SnF_4)$ @N1	-10006.737	-1.814
		$F(SnF_4)$ @H4	-10006.865	-1.942
		$F(SnF_4)$ @I5	-10006.974	-2.0507
		$F(SnF_4)$ @N1	-10006.924	-1.934
		$F(SnF_4)$ @H2	-10006.777	-1.853
SnI_2-T	Clean (010)		-7261.462	--
	SnF_2@clean (010) SnI_2-T	$F(SnF_2)$@I1	-8682.069	1.060
		$F(SnF_2)$@Sn4	-8681.582	1.5469
		$Sn(SnF_2)$@I1	-8681.991	1.1371
		$Sn(SnF_2)$@Sn4	-8682.084	1.044
	SnF_4@clean (010) SnI_2-T	$F(SnF_4)$ @ Sn4	-10005.252	1.7535

[a]The mark part in blue shows the most stable cases of every type.

to group VIIA, as well as the iodine atom, gaining electrons easily, leading to repulsion interaction. For (6), it is mainly because the F atom is more prone to forming a bond with the H atom of the NH_2 group than with the N atom. This is because the electronegativity difference[42] between the H atom (an electronegativity value of 2.1) and F atom (an electronegativity value of 4.0) is 1.9, whereas the electronegativity difference between the N atom (an electronegativity value of 3.0) and F atom is 1.0. The larger the electronegativity, the easier it is for two atoms to bond. Apart from four cases mentioned before, for SnF_4 molecule adsorption on the FAI-T surface, there are two cases that cannot be calculated successfully, which are (3) $Sn(SnF_4)$@H4@FAI-T and (4) $Sn(SnF_4)$@H2@FAI-T.

Similarly, for SnF_2 adsorption on SnI_2-T, there exist four cases in total: (1) $Sn(SnF_2)$@I1@SnI_2-T, (2)$Sn(SnF_2)$@Sn4@SnI_2-T, (3)$F(SnF_2)$@I1@SnI_2-T, and (4) $F(SnF_2)$@Sn4@SnI_2-T. All of the four cases were calculated successfully. In addition, for SnF_4 adsorption on the SnI_2-T surface, there are also four cases: (1) $Sn(SnF_4)$@I1@ SnI_2-T, (2) $Sn(SnF_4)$@Sn4@SnI_2-T, (3) $F(SnF_4)$@I1@SnI_2-T, and (4) $F(SnF_4)$@Sn4@SnI_2-T. There also exist a few cases that cannot be calculated for their misconvergence for SnF_4 molecule adsorption. Hence, finally, the case of $F(SnF_4)$@Sn4@SnI_2-T was successfully calculated, providing reasonable results. For the FAI-T surface, there are 10 cases that provided good results. Meanwhile, for the SnI_2-T surface, there are five cases. The total energies and the adsorption energies of clean surfaces and these adsorption cases are shown in Table 2. From Table 2, it is remarkable that the most stable condition for SnF_2 adsorption on the FAI-T surface is the case of $Sn(SnF_2)$@I5@FAI-T, denoted as S2. S1 refers to the case of a clean FAI-T surface. In addition, the most stable system for SnF_4 adsorption is the case of $F(SnF_4)$ @I5@FAI-T, noted as S3. S4 represents the case of a clean SnI_2-T surface. S5 denotes the most stable structure of the $Sn(SnF_2)$@Sn4@SnI2-T case. Finally, S6

https://doi.org/10.1021/acsomega.1c00767
ACS Omega 2021, 6, 14938−14951

represents the most stable structure for SnF_4 adsorption on the SnI_2-T surface, which is F(SnF_4)@Sn4@SnI_2-T. All in all, S1 is the clean (010) FAI-T surface, S2 is Sn(SnF_2)@I5@FAI-T, S3 is F(SnF_4)@I5@FAI-T, S4 is the clean (010) SnI_2-T surface, S5 is Sn(SnF_2)@Sn4@SnI_2-T, and S6 is F(SnF_4)@ Sn4@ SnI_2-T.

We find that the I5 position of FAI-T is the most active adsorption place from every model (S2, S3, S5, and S6) by the lowest-energy principle. Meanwhile, for SnI_2-T, it is the Sn4 atom that is the most active atom. In the aspect of the total energy of the system, the case of S2 = F(SnF_2)@I5@FAI-T has the smallest adsorption energy, which is 0.5376 eV, implying that the case of a F atom of SnF_2 molecule adsorption on the FAI-T surface has the most stable structure among all of the four adsorption cases.

In addition, we calculated the surface defect states, see Table S1 (Supporting information, SI). We studied various types of surface defects on three types of terminations, FAI, flat, and vacant, by first-principles calculations. Combining the calculated defect levels and the defect formation energy, our results can be summarized in three points as follows. (i) Under the I-rich condition, excess I atoms on flat and vacant surfaces are responsible for the carrier trapping. On the other hand, under the Sn-rich condition, I atom vacancies on vacant surfaces and excess Sn atoms on both flat and vacant surfaces act as carrier traps. (ii) The formation of carrier-trapping surface defects under the Sn-rich condition is thermodynamically more unfavorable than under the I-rich condition. (iii) Under the moderate condition, any surface defects that act as carrier traps have high formation energy, that is, cannot easily form the surface defect. From the above, to reduce carrier trapping on surfaces or grain boundaries so as to improve the carrier lifetime and avoid hysteresis, the Sn-rich condition is better than the I-rich condition.

3.2. Energy Band Structure and Effective Mass Analysis for Surface Adsorption. The band structures of the six cases (S1, S2, S3, S4, S5, and S6) are displayed in Figure 2. We used the PBE and SHE06 methods to calculate the energy band; the energy band calculated by this PBE is smaller than that by the SHE06 method (see the Supporting Information). By comparison, this SHE06 method is closer to the real value, according to the band structures calculated by the SHE06 method, and the electron's and hole's effective masses are calculated, shown in Table 3. From Figure 2, we notice clearly that after SnF_2 molecule adsorption on the FAI-T surface, the band gap (E_g) increases from 1.56 to 1.67 eV with an increase of 7%. However, for SnF_4 adsorption on the FAI-T surface, the E_g changes slightly, with an enhancement of 0.01 eV compared with the E_g of S1. For SnI_2-T surface adsorption, SnF_2 molecule adsorption also enlarges the E_g from 1.61 to 1.81 eV, with an increase of 12.4%. Meanwhile, SnF_4 molecule adsorption on SnI_2-T affects the E_g largely, which changes from 1.61 to 1.65 eV, with an increase of 2%. Moreover, there exist impurity levels in the cases of S3 of F(SnF_4)@I5@FAI-T and S6 of F(SnF_4)@Sn4@SnI_2-T. In S3, the impurity level is far away from the Fermi level (E_F) but close to the conduction band. In S6, the impurity level is located above the valence band and close to the Fermi level. It was obvious that the SnF_2 molecule broadened the band gap more greatly after adsorption on the two surfaces than the SnF_4 molecule did. However, the SnF_4 molecule induced impurity levels to the FAI-T surface and SnI_2-T surface, and

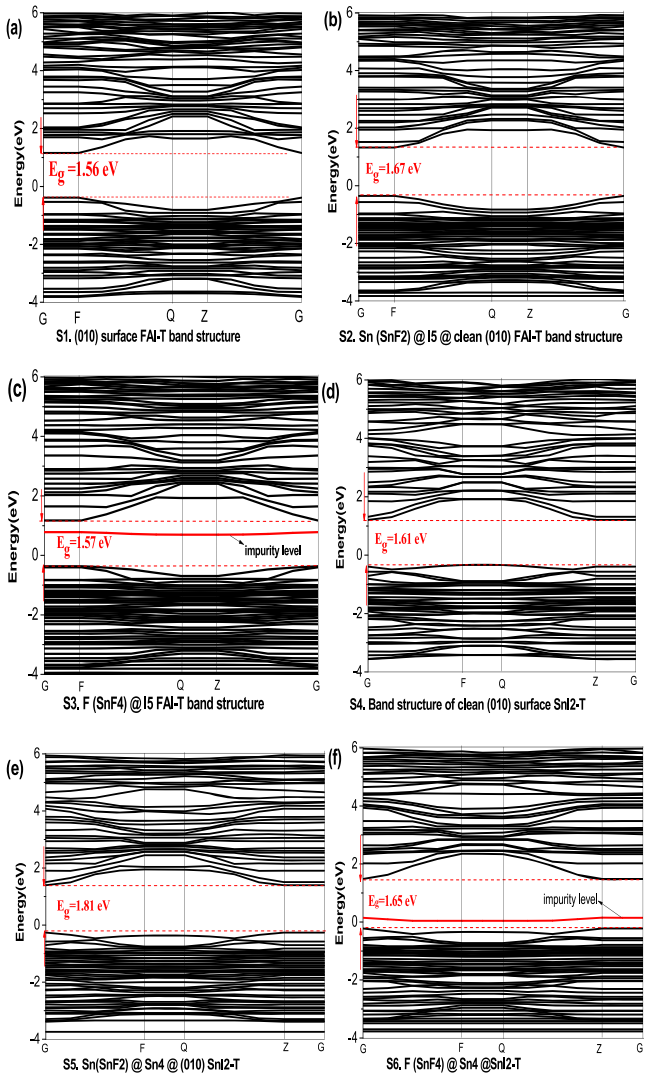

Figure 2. Band structures of (a) S1, clean (010) FAI-T surface; (b) S2, Sn(SnF_2)@I5@ FAI-T; (c) S3, F(SnF_4)@I5@FAI-T; (d) S4, clean(010)SnI_2-T surface; (e) S5, Sn(SnF_2)@Sn4@SnI_2-T; and (f) F(SnF_4)@Sn4@SnI_2-T. The red solid line stands for the impurity level in panels (c) and (d).

the p-type semiconductor characteristics of these surfaces did not change.

Additionally, as we all know, the band structure relates to the distribution of electrons and holes. Why do SnF_2 molecules enlarge the band gap of the FAI-T surface and SnI_2-T surface? We consider that the SnF_2 adsorption on the two surfaces eliminates effectively more dangling bonds of these unsaturated coordinated atoms on the surfaces, which affect the energy distribution of surface defect states, leading to the bottom of the conduction band rising up and keeping the top of the valence band unchanged relative to the Fermi level, then resulting in the increase in the band gap. Then, based on band structures, we calculated the electron effective masses (m_e^*) and the hole effective masses (m_h^*).

Since the slope of the band edge is associated with the effective mass of carriers, the electron transfer along the *a* and *b* directions should be more favorable than along the *c* direction. We can calculate the effective mass of charge carriers by the shape of the energy band, as shown in the following equation:

https://doi.org/10.1021/acsomega.1c00767
ACS Omega 2021, 6, 14938−14951

Table 3. Band Gaps, Lattice Parameters, and Electron or Hole Effective Masses of S1, S2, S3, S4, S5, and S6

Case	Eg/eV	Lattice Parameters			Effective mass(m*)	
		a/Å	b/Å	c/Å	The effective mass of electrons (m^*_e/m_0)	The effective mass of holes (m^*_h/m_0)
S1. (010) FAI-T surface	1.157	8.818	23.842	8.857	F-Q: 0.301, Z-G: 0.256 (0.279)	F-Q: -0.564, Z-G: - 0.349 (- 0.457)
S2. Sn(SnF_2)@I5@FAI-T	1.289 (+11.4%)	8.818	23.842	8.857	F-Q: 0.231, Z-G: 0.217 (0.224)	F-Q: - 0.384, Z-G: - 0.393 (- 0.389)
S3.F(SnF_4)@I5@FAI-T	1.167 (+0.8%)	8.818	23.842	8.857	F-Q:0.287, Z-G: 0.232 (0.260)	F-Q: - 0.577, Z-G: -0.752 (- 0.665)
S4. clean(010) SnI_2-T	1.205	8.857	8.818	21.492	G-F: 0.394, Q-Z: 0.305 (0.350)	G-F: - 0.477, Q-Z: - 0.786 (- 0.632)
S5. Sn(SnF_2)@Sn4@SnI_2-T	1.398 (+16.0%)	8.857	8.818	21.492	G-F: 0.166, Q-Z: 0.200 (0.183)	G-F: - 0.500, Q-Z: - 0.461 (- 0.481)

[a]Characters in blue in the brackets are the average values of effective masses of electrons and holes.

$$m^* = \hbar^2 \left[\frac{\partial^2 \varepsilon(k)}{\partial k^2} \right]^{-1} \quad (5)$$

where $\varepsilon(k)$ is the average eigenvalue of the band, k is the wavevector, m^* is the charge carrier effective mass (m_e^* and m_h^* are the electron and hole effective masses, respectively), and the results are shown in Table 3. In Table 3, for FAI-T surface adsorption, both SnF_2 and SnF_4 molecules reduce their m_e^*. In S2, the SnF_2 molecule reduces the average m_e^* from 0.279 to $0.224m_0$ and reduces the average m_h^* from −0.457 to $-0.389m_0$ too. As for S3, the average m_e^* decreases to $0.260m_0$, along with m_h^* increasing to $-0.665m_0$. Apparently, the reduced ratio of m_e^* of SnF_2 adsorption is greater than that of SnF_4 adsorption on the FAI-T surface.

Similarly, for SnI_2-T surface adsorption, both SnF_2 and SnF_4 have decreased m_e^* and m_h^* after adsorption on the SnI_2-T surface. For S5, the SnF_2 molecule made the average m_e^* decrease from 0.350 to $0.183m_0$, with m_h^* decreasing from −0.632 to $-0.481m_0$. Surprisingly, for S6, m_e^* is essentially unchanged in $0.316m_0$, and m_h^* reduces to $-0.625m_0$.

Based on the effective mass results, SnF_2 adsorption clearly reduces the carrier effective masses of the two surfaces. SnF_4 reduces the carrier effective masses (electron and hole) of SnI_2-T and the electron effective mass of FAI-T but raises the hole effective mass of FAI-T. It can be concluded that SnF_2 is a powerful additive for $FASnI_3$ to promote charge transfer.

Whether they are adsorbed on the FAI-T surface or on the SnI_2-T surface, the fluoride additives (SnF_2 and SnF_4) enlarge the band gaps in all four cases and decrease the carrier effective masses (m_e^* and m_h^*) except for S3. Furthermore, SnF_2 has a more powerful ability to broaden the band gap and to decrease the effective mass of electrons and holes than that of SnF_4. Except from those mentioned above, two impurity levels catch much attention. In S3, the F atom of SnF_4 is adsorbed at the I5 atom of the FAI-T surface, and an impurity level below the conduction band and above the Fermi level emerges, which is shown in Figure 2c (see the red line). Coincidently, an impurity level emerges as well in S6 for SnF_4 adsorption on the SnI_2-T surface, as shown in Figure 2f (see the red line). In S6, the impurity level in the band gap is close to the conduction band and is away from the valence band. However, it weakens the m_h^*, differing from that of S3, in which the m_h^* was enhanced. It is well known to all that when the electrons in the valence band jump to the conduction band, it first jumps to the nearby impurity energy level rather than transferring to the conduction band. Thus, the impurity energy level will maybe become a recombination center, and binding the electron, leading to a decrease of the effective mass of the carrier. In addition, for SnF_2 molecule adsorption on the FAI-T or SnI_2-T surface, the energy levels of SnF_2 are located in the valence band. These energy levels have strong interactions with the levels below the valence band, decreasing the hole effective mass. Therefore, with regard to the band structure and the carrier effective mass, SnF_2 is superior to SnF_4 in enhancing the charge transfer for $FASnI_3$.

In pursuing high-performance PSCs, the small effective mass contributes to bigger carrier mobility.[43−45] By this point, the SnF_2 molecule affected the two surfaces positively in terms of relieving the carrier effective mass. To specify the interactions between different adsorbates and the surface, the electron density distributions are depicted in the density of states (DOSs) in later paragraphs.

3.3. Density of States and Partial Density of States for Surface Adsorption. To explore the electronic structures of the two surfaces after SnF_2 and SnF_4 adsorption, the total density of states (TDOS) and the partial density of states (PDOS) of all the six cases (S1, S2, S3, S4, S5, and S6) were calculated, as shown in Figure 3a−f corresponding to the DOSs of S1, S2, S3, S4, S5, and S6, respectively.

For the clean FAI-T surface, as shown in Figure 3a, the peak of the TDOS of S1 is located at −1.5 eV. There are three lower subpeaks in the valence band located at −2, −2.7, and −3.8 eV. From Figure 3a, it is obvious that the TDOS from −3 eV to 0 is mainly contributed by the Sn 5p orbital and I 5p orbital electrons. At −2 eV, the PDOS of the I 5p orbital shows a sharp peak, indicating that I 5p orbital electrons possess a strong electronic localization property.[46−48] In the conduction band above Fermi level, there appears two peaks from 0 to 3 eV. One peak is at 1.9 eV, and another peak is located at 2.5 eV. The peak of the TDOS is contributed by the FA 2p orbital, Sn 5p orbital, and I 5p and I 5s orbital electrons. The peak of the PDOS of the Sn element is at 2 eV, and the subpeak is at 1.2 eV.

https://doi.org/10.1021/acsomega.1c00767
ACS Omega 2021, 6, 14938−14951

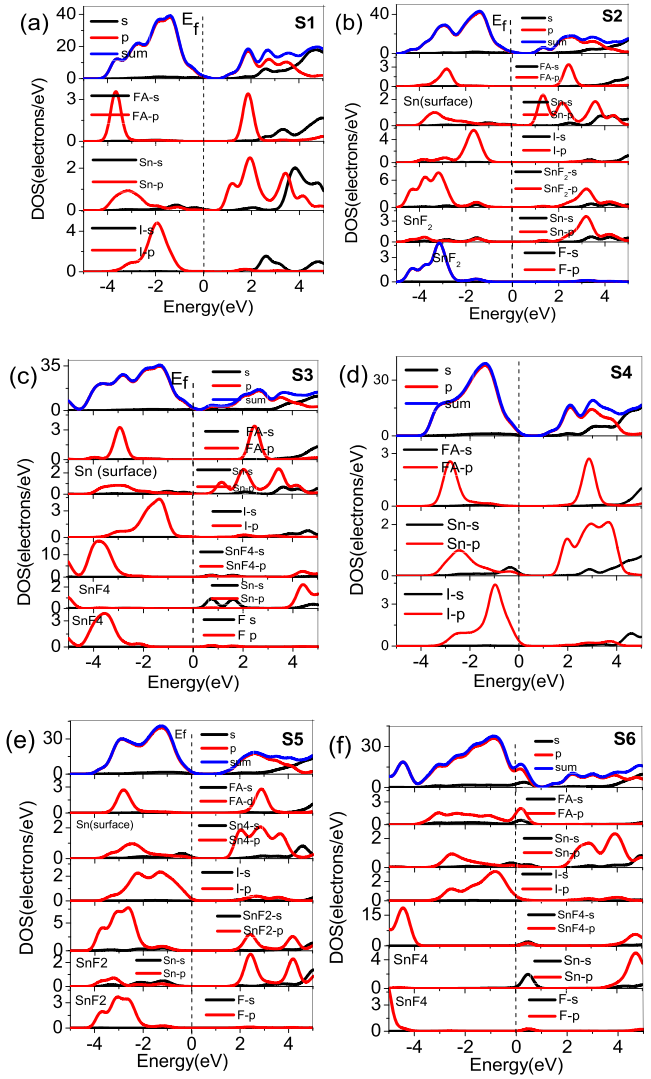

Figure 3. Density states of (a) S1, clean (010) FAI-T; (b) S2, $Sn(SnF_2)$@I5@FAI-T; (c) S3, $F(SnF_4)$@I5@FAI-T surface; (d) S4, clean(010)SnI_2-T surface; (e) S5, $Sn(SnF_2)$@Sn4@SnI_2-T surface; and (f) S6, $F(SnF_4)$@Sn4@SnI_2-T surface.

After SnF_2 molecule adsorption on the FAI-T surface, as shown in Figure 3b, the TDOS alters dramatically. In Figure 3b, the main sharper peak of the TDOS is at −1.4 eV, accompanied by a subpeak at −3 eV. In addition, the DOSs of the FA cation shifts toward the right. For the PDOSs of the Sn atom and I atom, the curves change greatly. The peak of Sn's PDOS is located at 1.3 eV with an increased peak. However, SnF_2 molecule adsorption makes the PDOS of the I atom diffuse. Before SnF_2 adsorption on FAI-T (seeing Figure 3a), not only does a peak at −2 eV exist, along with a subpeak at −3 eV in the valence band, but also a new third weak peak at −4 eV emerges. In addition, after SnF_2 adsorption on FAI-T, the Sn atom originates from SnF_2 adsorbed at the I5 atom of FAI-T, resulting in the overlapping electron cloud between the I 5p orbital and Sn 5s and 5p orbitals in the range from −4 to −1 eV. The result indicates that the I atom had strong interaction with the Sn atom of SnF_2, forming a Sn−I bond, which broadened the band gap and elevated the conduction band. The results agree with Figure 2.

When the SnF_4 molecule adsorbed on FAI-T (see Figure 3c), the TDOS showed a long span peak from −1.2 to −2 eV, indicating that the delocalization property of electrons increases after SnF_4 adsorption. In addition, the PDOS of Sn in this diagram has a flatter peak than those of S1 and S2 in the valence band, meaning that the PDOS peak of the I atom moved toward the Fermi level, showing that the SnF_4 molecule makes great contributions to the TDOS constitution in the valence band.

Comparing the DOSs of S2 and S3 with that of S1, both DOS curves of S2 and S3 move to the right. Apart from this, the PDOS curves of the Sn atom of S1, S2, and S3 differ from each other distinctly, especially the curves' shapes in the valence band. A proof is the sharpness of the peak of the PDOS of the Sn atom on the FAI-T surface. In Figure 3a−c, SnF_2 adsorption makes this peak sharper than that of S1, while SnF_4 adsorption makes it flatter with a long span. These different phenomena show that the distribution of the Sn atom on the FAI-T surface is highly localized after SnF_2 molecules adsorbed, while SnF_4 molecules make it more diffuse. In other words, SnF_2 molecules make the electrons of Sn on the FAI-T surface localized, but SnF_4 molecules make them delocalized. Localized electrons build up strong bonds, while delocalized electrons weaken the bond. Hence, adding SnF_2 molecules contribute to the bond strength of Sn−I, while SnF_4 molecules decrease the Sn−I bond strength. Therefore, SnF_2 molecule adsorption has a deeper influence on the FAI-T surface than SnF_4 molecule adsorption. For the SnI_2-T surface, the DOSs of the three cases (clean SnI_2-T surface, SnF_2 adsorption, and SnF_4 adsorption) are shown in Figure 3d−f, respectively.

For the clean SnI_2-T surface, the peak of TDOS is located at −1.5 eV, with a subpeak at −3.2 eV. For the PDOS of the FA cation, it has no electrons distributed near the Fermi level, and it has two peaks, which is distributed symmetrically in the valence band and in the conduction band. For the PDOS of the Sn atom, it presents a peak at −2.5 eV in the valence band, along with a smaller peak close to the Fermi level, and the PDOS at the Fermi level does not reach a value of 0. For the PDOS of the I atom, a sharp peak at −1 eV appears, with a flat peak at −2.5 eV.

When SnF_2 adsorbs on the SnI_2-T surface, the TDOS and PDOSs alter apparently (see Figure 3e). For the TDOS, after SnF_2 adsorbed, the enhanced subpeak originally at −3.2 eV shifts to the right to 3 eV. In the conduction band, a peak at 1 eV and another at 2 eV disappeared, with a new peak at 1.5 eV for the PDOS emerging. The PDOS of FA does not change. For the PDOS of the Sn atom, the electron distribution in the valence band gets more diffuse toward the low-energy direction. More interestingly, the PDOS of the I atom alters dramatically. Compared with the PDOS of the I atom in Figure 3d,e, one sharp peak at −1 eV and another lower peak at −2.5 eV originally shift to a peak at −1.5 eV and a peak at −2.3 eV, respectively. SnF_2 molecule adsorption on SnI_2-T changes the electron distribution of nearby I atoms hugely. In addition, there exists an overlap of PDOSs between the adsorption location of the Sn4 atom on SnI_2-T and the Sn atom of SnF_2 from −4 to 0 eV, with the overlap between the Sn 5p orbital of the surface and the Sn 5s and 5p orbitals of SnF_2. The phenomenon indicates that the repulsive interaction between two Sn atoms belongs to the surface and SnF_2, forming a Sn−Sn bond. Hence, the Sn−Sn bond heightens the conduction band, with the band gap enlarged.

For SnF_4 adsorption on the SnI_2-T surface, the most interesting point is that at the Fermi level, the TDOS does not reach 0. At the Fermi level, the PDOS consists of the PDOS of

https://doi.org/10.1021/acsomega.1c00767
ACS Omega 2021, 6, 14938−14951

Table 4. Parameters of Bonds Formed between the Adsorption Location of the Surface and the Atom of SnF_2 or SnF_4 with Related Parameters of Clean Surfaces and Free Fluorides (SnF_2 and SnF_4)

Case	Parameters			
	Bond	Bond length/Å	Bond angle/°	Atom--charge/e
S1. clean FAI-T	--	--	--	I5-- -0.48
	Sn5—I5	3.058	--	Sn5—0.99, I5 -- - 0.31
S2. Sn(SnF_2)@I5 FAI-T	I5—Sn5—F2	--	96.001	
	I5—Sn5—F2	--	94.063	
	F(SnF4)—I5	3.241	--	Sn5—1.88, I5 -- - 0.17, F3 -- -0.63
S3. F(SnF_4)@I5@FAI-T	I5—Sn5—F3	--	90.563	
	F1—Sn5—F1	--	86.793	
S4. Clean SnI_2-T	--	--	--	Sn4– 0.48
	Sn4—Sn5	3.617	--	Sn4—0.43, Sn5—1.05
S5. Sn(SnF_2)@Sn4@SnI_2-T	Sn4—Sn5—F2	--	151.365	
	Sn4—Sn5—F51	--	102.688	
	Sn4—F4	2.278	--	Sn4—0.70, F4 -- - 0.58
S6. F(SnF_4)@Sn4@SnI_2-T	F2—Sn5—F1	--	92.709	
	F1—Sn5—F3	--	94.300	
Free SnF_2 molecule	--	--	--	Sn—1.25, F—0.62/0.63
Free SnF_4 molecule	--	--	--	Sn—2.30, F1/2-- -0.55, F3/4 -- -0.60

[a]The bond in blue indicates the newly formed bond between the adsorbate and the adsorption location of the perovskite surface.

FA, that of Sn on the SnI_2-T surface, and that of the I atom. As shown in Figure 3f, the Fermi level enters into the valence band, forming a degenerate state.[49−52] This makes the top of the valence band generate excess hole carriers for SnF_4 adsorption on the SnI_2-T surface. SnF_4 adsorption made the SnI_2-T surface exhibit p-type semiconductor characteristics. Combined with the corresponding band structure of this case, shown in Figure 2f, SnF_4 molecule adsorption on SnI_2-T generates an impurity level in the valence band under the Fermi level. Based on the related PDOS diagram, the impurity level consists of FA 2p orbital and F 2p orbital electrons. As shown in Figure 3f, though the TDOS of S6 increases after SnF_4 molecules adsorbed, the PDOS of FA diffuses. So did the PDOS of the Sn atom close to the SnF_4 molecule. Zhou's group[53] suggested that the F atom of fluorides formed a N−H···F hydrogen bond between the F atom and organic cation. Our results of the DOS and PDOS agree with their experimental results. According to Figure 3f, after SnF_4 adsorption, the discrete distribution of FA's PDOS becomes continuous, implying the charge transfer from the FA cation to the adjacent SnF_4 molecule. As we all know, FA ($H_2N−CH═NH_2$) possesses an extra proton in one NH_2 part, bonding with the F atom easily. Additionally, the PDOS of the Sn atom adsorbed on the SnF_4 molecule moves to the right slightly, so that there exist a few electrons distributed at the Fermi level. The PDOS of the I atom shifts toward the right as well, leading to the denser distribution of electrons near the Fermi level.

Similar to the comparison among the three cases of the FAI-T surface, here, we compare the DOS and PDOS of the SnI_2-T surface for S4−S6 based on Figure 3d−f, respectively. SnF_2 molecules supported electrons mainly in the range from −4 to −2 eV. However, SnF_2 does not affect the electron distribution of the FA cation, indicating that the SnF_2 molecule has no interaction with the FA cation. Additionally, SnF_2 adsorption on this surface boosts the Sn−I bond of the surface, enhancing the binding force with the SnI_2-T surface. Meanwhile, for SnF_4 molecule adsorption on this surface, the interaction between the FA cation and F atom is so strong that the PDOS of FA altered obviously. In addition, SnF_4 contributes electrons to the surface in the range of −5 to −4 eV and in the range of 0 to 1 eV. In Figure 3f, the peak at E_F is contributed by FA 2p orbital electrons, Sn 5s and 5p orbital electrons of the SnI_2-T surface, I 5p orbital electrons, Sn 5p orbital electrons of SnF_4, and F 2p orbital electrons. In this case, SnF_4 forms a hydrogen bond between FA and the F atom, stabilizing the structure in a heated environment. Additionally, the electronic valence state

https://doi.org/10.1021/acsomega.1c00767
ACS Omega 2021, 6, 14938−14951

Table 5. Bond Lengths of the Sn−I Bond in S1, S2, S3, S4, S5, and S6

Case	Bond length of Sn—I bond
S1. clean FAI-T surface	2.976, 2.977, 2.9927, 2.9927, 2.9847 (2.9847)
S2. Sn(SnF_2)@I5@FAI-T	2.9307, 2.931, 2.966, 2.991, 2.955 (2.955, -0.99%)
S3. F(SnF_4)@I5@FAI-T	2.976, 2.976, 2.992, 2.992, 2.984 (2.984, 0%)
S4. clean SnI_2-T surface	2.903, 2.905, 2.954, 2.955, 2.929, 2.929 (2.929)
S5. Sn(SnF_2)@Sn4@SnI_2-T	2.912, 2.969, 2.949, 2.951, 2.945 (2.945, +0.56%)
S6. F(SnF_4)@Sn4@SnI_2-T	2.892, 2.890, 2.975, 2.979, 2.934 (2.934, +0.17%)

[a]The first character in blue in brackets stands for the mean value. The percentage is relative to the clean surface.

of Sn in the SnF_4 molecule is $4d^{10}5s^05p^0$. However, it is the Sn 5s orbital electron state that contributes to the TDOS, indicating that the 5s orbital of Sn in the SnF_4 molecule has accepted electrons from other atoms. Thus, the Sn^{4+} ion of SnF_4 acts as a shallow acceptor.

Therefore, from Figure 3, we conclude that the adsorbed SnF_2 molecules form different new bonds with the FAI-T surface and SnI_2-T surface, for instance, the Sn−I bond and the Sn−Sn bond. These new bonds passivate the perovskite's surface effectively and hinder the charge transport between the SnF_2 molecule and the surface of the perovskite. Additionally, based on the DOS, in F(SnF4)@Sn4@SnI_2-T, the strong hydrogen bond N−H···F facilitates the thermal stability of perovskite solar cell devices. Also, for the SnI_2-T surface, a small amount of SnF_4 generated less impurity bands near the Fermi level above the valence band. The impurity band may become a new recombination center when the amount of SnF_4 molecules increases. As for the FAI-T surface, the impurity level is located below the conduction band and away from the Fermi level after SnF_4 adsorption. As a result, it accepts more electrons that jumped from the impurity levels. The impurity level will become a new recombination center. Therefore, SnF_2 molecule adsorption increased the band gaps of both surfaces greatly compared to SnF_4 molecule adsorption, while SnF_4 adsorption on both surfaces induced impurity levels, making them a new recombination center and hindering the carrier transfer process.

3.4. Bond Analysis on Surface Adsorption. Bond analysis is necessary for studying the energy transduction because the DOS cannot display the real space distance and energy state between related atoms. In this part, we discuss three cases. They form the bonds between an atom of the SnF_2 or SnF_4 molecule and an atom on the surface. We found that the Sn−I bond and Sn−F bond play a crucial role in the structural stability of $FASnI_3$. For example, the Sn−I bond belongs to the perovskite surface, and the Sn−F bond belongs to the SnF_2 or SnF_4 molecule. The related parameters, such as bond lengths, bond angles, and charges, are shown in Table 4. As shown in Table 4, the Sn5 atom comes from the SnF_2 molecule and the F atom is from the SnF_4 molecule, which form the Sn5−I5 bond and F−I5 bond with the FAI-T surface atoms, respectively. These bonds eliminate the coordinationally unsaturated states of the I5 atom on FAI-T. The bond length of the Sn5−I5 bond is 3.058 Å. The bond length of the F−I5 bond is 3.241 Å. These results indicate that on the clean FAI-T surface exist the unsaturated I atoms with dangling bonds and unpaired electrons. On the SnI_2-T surface, the Sn4 atom of SnI_2-T bonds with the Sn5 atom of the SnF_2 molecule, forming a Sn4−Sn5 bond.

In addition, there exists a charge transfer behavior between the SnF_2 or SnF_4 molecule and some atoms on the perovskite surface. For the FAI-T surface, the I5 atom catches much attention in the aspect of charge transfer and becomes a better adsorption location on the surface for SnF_2 and SnF_4 adsorption on the FAI-T surface. In S2, the I5 atom and Sn5 atom have charges of $-0.31e$ and $0.99e$, respectively. Compared with the charges of S1, the obtained charges for the I5 atom and Sn5 atom are $0.17e$ and $0.26e$, respectively. In S3, the I5 atom, the F3 atom, and the Sn5 atom have charges of $-0.17e$, $-0.63e$, and $1.88e$, respectively. Compared with those of S1 and free SnF_4 molecules, the I5 atom gains a $0.31e$ charge, the F3 atom loses a $0.03e$ charge, and the Sn5 atom loses a $0.42e$ charge. In S5, the Sn4 atom and the Sn5 atom have charges of $0.43e$ and $1.05e$, respectively. In this case, after SnF_2 adsorption, the Sn4 atom and the Sn5 atom lose $0.05e$ and $0.20e$ charges, respectively. In S6, the Sn4 atom and the F4 atom possess charges of $0.70e$ and $-0.58e$, respectively. Compared with those of S4 and free SnF_4 molecules, the Sn4 atom gains a $0.22e$ charge and the F4 atom loses a $0.02e$ charge. From the above, we know they can lose or gain different amounts of electrons in different circumstances, and combining with the bond length of Sn4−F4, the charge transfer happens between the Sn4 and F4 atom. The obvious short bond length of Sn4−F4 is a strong ionic bond and indicated the dramatic change in electron distribution, corresponding to the DOS of S6.

As shown in Table 5, for S2, the average bond length of the Sn−I bond of the perovskite surface decreases from 2.984 to 2.955 Å with a decrease of 0.99%. In S3, the average bond length of Sn−I is 2.984 Å, without any changes, indicating that the SnF_4 molecule has a weak interaction with the perovskite surface and even reflecting how the SnF_4 molecule adsorption hardly affected the structural stability of FAI-T. The cases of SnF_2 and SnF_4 adsorption on the SnI_2-T surface have a few differences. In S5, the average bond length of Sn−I increases from 2.929 to 2.945 Å with an increase of 0.56%. For the S6 model, the average bond length of Sn−I increases to 2.93406 Å too, with an increase of 0.17%.

From Table 5, apparently, SnF_2 is able to shorten the bond length of Sn−I, indicating that SnF_2 is beneficial to strengthening the Sn−I bond of the FAI-T surface. Compared with the effect of SnF_2 adsorption on the FAI-T surface, SnF_4

https://doi.org/10.1021/acsomega.1c00767
ACS Omega 2021, 6, 14938−14951

Table 6. Bond Lengths of the Sn−F Bond of Free SnF_2 and SnF_4 Molecules and of S2, S3, S5, and S6

Case	Bond length of Sn—F bond/Å
SnF_2 molecule	2.0539, 2.0966, 2.114, 2.195, 2.348, 2.4331, 2.516, 2.054, 2.348, 2.195, 2.433 (2.085)
SnF_4 molecule	2.079, 1.950, 2.079, 1.950, 2.079, 2.079 (2.036)
S2. Sn(SnF_2)@I5@FAI-T	2.036, 2.065 (2.050, -1.64%)
S3. F(SnF_4)@I5@FAI-T	1.961, 1.999, 2.011, 2.016 (1.996635, -1.93%)
S5.Sn(SnF_2)@Sn4 @SnI_2-T	2.013, 2.026 (2.0195, -3.12%)
S6. F(SnF_4)@Sn4@SnI_2-T	2.025, 1.982, 2.015, 2.064 (2.022, -0.70%)

[a]The first character in blue in brackets stands for the mean value. The percentage is relative to the clean surface.

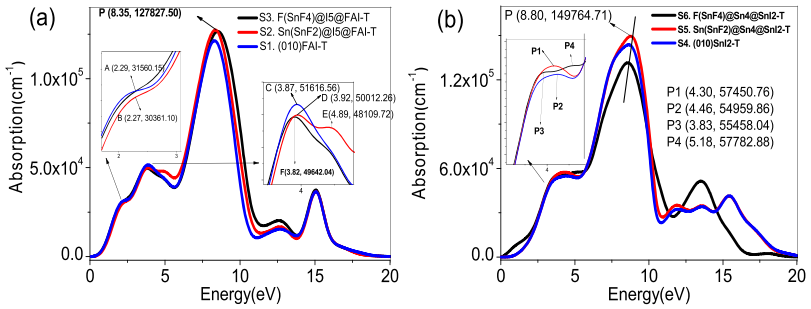

Figure 4. Absorption curves of (a) three cases of the FAI-T surface and (b) three cases of the SnI_2-T surface.

adsorption on the FAI-T surface sustains the bond length of the Sn−I bond. As for the other surface of SnI_2-T, SnF_2 and SnF_4 both increase the average bond length of the Sn−I bond. Additionally, the increase of S5 is larger than that of S6, meaning that SnF_2 affects the SnI_2-T surface greatly compared to SnF_4. Therefore, SnF_2 affects the two surfaces largely, either by shortening the bond length of Sn−I on the FAI-T surface or by enlarging the bond length on the SnI_2-T surface. Especially, SnF_2 adsorption strengthens the bond length of the Sn−I bond of the FAI-T surface, which is distinct from SnF_4 molecule adsorption. At this point, SnF_2's performance is superior to that of SnF_4. Nevertheless, the oxidized products of SnF_2 and SnF_4 can maintain the bond strength of the Sn−I bond on the FAI-T surface with a slight variation on the SnI_2-T surface. Thus, a conclusion is drawn: SnF_2 is able to enhance the Sn−I bond of the perovskite surface, increasing $FASnI_3$'s photoelectric properties.

Another important bond is the Sn−F bond. The Sn−I bond of the surface affects not only the stability and photoelectric properties but also the properties of perovskite. Table 6 shows the bond lengths of the Sn−F bonds of the free SnF_2 and SnF_4 molecules and of S2, S3, S5, and S6. From Table 6, in the S2 case, the average bond length of the Sn−F bond decreases from 2.085 to 2.050 Å with a decrease of 1.64%. In the S3 case, the average bond length decreases from 2.036 to 1.997 Å with a decrease ratio of 1.93%. In the S5 and S6 cases, the average bond length of the Sn−F bond reduces from 2.085 to 2.0195 Å with a decrease of 3.12% and reduces from 2.036 to 2.022 Å with a decrease of 0.70%, respectively. These results indicate that these fluorides adsorbed on the perovskite surfaces form a strengthened Sn−F bond.

Through the analysis of the band structures and DOSs, we notice that the SnF_4 molecule adsorbed on FAI-T changes the band gap slightly, and the bond length of the Sn−I bond almost does not alter. This denotes that SnF_4 molecule adsorption has no effect on the FAI-T surface. However, SnF_4 improves the DOS greatly near the Fermi level in S6. It forms a strong Sn4−F4 bond in S6. The F atom of SnF_4 has a strong interaction with the Sn4 atom with charge transfer. As a result, the Sn4−F4 bond weakens the bond strength of the Sn−I bond of the surface, producing an unstable state on the surface. Therefore, SnF_4 has no positive effect on the SnI_2-T surface.

Additionally, from the point of view of atomic coordination, the I atom of FAI-T is in an unsaturated state. As for the SnI_2-T surface, both the Sn atom and I atom are both not saturated. Therefore, the I atom of FAI-T, the Sn atom, and the I atom of SnI_2-T all have dangling bonds. As we all know, the Sn^{4+} cation has a higher stability than the Sn^{2+} cation,[54−56] and both of them have stable $[SnI_6]^{4-}$ octahedral strucutres.[57] When the Sn atom of SnF_2 adsorbs at the Sn4 atom of SnI_2-T, in S5, a Sn−Sn bond is formed. On the other hand, the F atom of SnF_4 adsorbs at Sn4 in S6, forming the F−Sn bond. The passivation effect of SnF_2 is better than that of SnF_4, producing more dangling bonds of SnF_2 than of SnF_4. In addition, the radius of Sn^{2+} is 1.12 Å, larger than the radius of Sn^{4+} (0.69 Å). The I atom is coordinated with Sn^{4+}, such as in the case of S3. This may induce the instability of perovskite because of the difference in particle sizes of Sn^{2+} and Sn^{4+}. Hence, the SnF_2 molecule has a more positive effect on the perovskite surface in terms of saturating uncoordinated atoms of the two surfaces than SnF_4.

https://doi.org/10.1021/acsomega.1c00767
ACS Omega 2021, 6, 14938−14951

3.5. Optical Absorption Properties. The formula of the absorption coefficient is shown by eq 3. The absorption curves of the six cases are sketched in Figure 4. Figure 4a represents the absorption curves of clean FAI-T and SnF_2 adsorption and SnF_4 adsorption on the FAI-T surface, respectively. Figure 4b represents the absorption curves of clean SnI_2-T and SnF_2 adsorption and SnF_4 adsorption on the SnI_2-T surface.

Figure 4 shows that the SnF_2 molecule promotes the adsorption performance of perovskite whether it occurs on the FAI-T surface or on the SnI_2-T surface. In Figure 4a, the peak of the absorption coefficient of SnF_2 adsorbed on FAI-T is 127,827.50 cm^{-1}, which is the highest peak among all three cases (S1, S2, and S3). In addition, the absorption peaks and absorption edges are both shifted toward a higher-energy direction with a blue shift. In Figure 4b, the maximum absorption coefficient comes from the SnF_2 adsorption on SnI_2-T, which is 149,764.71 cm^{-1}. The locations of absorption peaks in these three cases are nearly the same, but the absorption edges shift toward the higher-energy direction too.

Coincidental with the DOS analysis, here, we just discuss the cases in a low-energy distribution range from 0 to 5 eV. In the range of 0 to 5 eV, a new absorption peak at 4.89 eV for SnF_2 adsorption on the FAI-T surface appears, while SnF_4 adsorption on the same surface does not lead to a unique peak. Combined with Figure 3, from 0 to 5 eV, the absorption curves of the clean FAI-T surface and the SnI_2-T surface are distinct because of the different elemental components. In Figure 4a, in the range from 0 to 5 eV, the curve of the clean FAI-T surface has two clear peaks. The curve of SnF_4 adsorption on FAI-T also has two peaks at the same energy level compared with that of the clean FAI-T surface. However, SnF_2 adsorption on FAI-T showed a third peak at 4.89 eV aside from the two other peaks at the same positions (2.27 and 3.82 eV). The peaks are related to the charge transfer process, based on the DOS of Figure 3b. The third peak (at 4.89 eV for SnF_2 adsorption on FAI-T, in Figure 4a) is attributed to the electron transfer from the Sn 5s orbital to the F 2p orbital, both of which come from the SnF_2 molecule. The result indicates that the internal charge transfer of the SnF_2 molecule causes a new absorption subpeak. However, this process does not contribute to the carrier transfer of perovskite. In Figure 4a, the absorbance curve of S3 did not show peaks at this energy level, which reveals that the Sn5−I5 bond plays an important role in boosting the second absorption in S2. For the SnI_2-T surface, in the range of 0 to 5 eV, there are many differences of absorption peak. From 0 to 5 eV, S5 has the highest peak at 4.30 eV, as shown by P1. Meanwhile, S6 has a peak at 4.46 eV, as shown by P2. A weak absorption peak indicates a forbidden transition. Therefore, the SnF_4 molecule adsorption is predicted to hinder the charge transition on the two surfaces, while for SnF_2 molecule adsorption, the opposite is concluded.

3.6. Dielectric Function. Figure 5 shows the dielectric functions of the six cases. According to the Fermi gold rule[58] and the definition of direct transition, ε_2 is described as the formula below

$$\varepsilon_2(q \to O_u, \hbar\omega) = \frac{2e^2\pi}{\Omega\varepsilon_0} \sum_{K,V,C} |\langle\psi_K^C|\vec{\mu}\cdot\vec{\gamma}|\psi_K^V\rangle|^2 \times \delta(E_K^C - E_K^V - E) \quad (6)$$

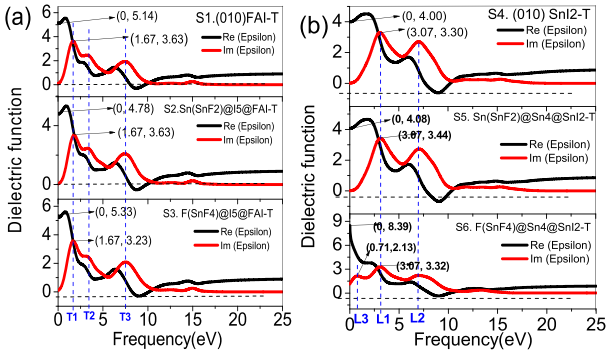

Figure 5. Dielectric function curves of (a) three cases of FAI-T and (b) three cases of SnI_2-T.

In the formula above, μ is the polarization direction vector of the incident electric field. V and C represent the valence band and conduction band, respectively. K is the reciprocal lattice vector. The component $\langle\psi_K^C|\mu\rightarrow \cdot \gamma\rightarrow|\psi_K^V\rangle$ stands for the momentum transition matrix. E_K^C and E_K^V stand for the intrinsic level of the conduction band and the valence band, respectively. It just takes electron transition into consideration in CASTEP. Thus, the dielectric function can be described as a linear response function. The distribution of the peak of the imaginary part is related to the electronic structure. At a frequency of 0 point, the value of ε_1 is the static dielectric constant, which just considers the electron polarization. In addition, the highest peak of ε_1 is caused by the electron transition from the top of the valence band to the bottom of the conduction band.

For the dielectric function, we focus on the energy range from 0 to 5 eV. In Figure 5a, the curves of ε_2 in the FAI-T surface have similar characteristics with regard to the three peaks and two other subpeaks at the same frequency levels. For example, the frequency levels of T1, T2, and T3 (at 1.67, 3.28, and 7.51 eV) do not shift, indicating SnF_2 and SnF_4 molecule adsorption on FAI-T did not affect the charge transition in the range of 0 to 5 eV. However, for the ε_1 curve of S2, the static dielectric constant reduces slightly from 5.14 to 4.78. The static dielectric constant of S3 increases to 5.33. For the FAI-T surface, the static dielectric constant does not change the polarization property. The result shows that the FAI-T surface possesses good stability when SnF_2 or SnF_4 adsorbed on this surface.

Similarly, in Figure 5b, on the SnI_2-T surface, for the ε_2 curves in the three cases, there are two differences in the curves of S4, S5, and S6: the intensity and the number of peaks. As shown in Figure 5b, the photon energy levels of the peak and a subpeak (3.07 eV for L1 and 7.03 eV for L2) do not change after SnF_2 and SnF_4 adsorption. However, the subpeak L2 is more nonlocalized than the two other peaks in the S4 and S5 cases. Additionally, the third peak L3 is at 0.71 eV. Compared with the energy band structure, we guess that the third peak originated from the transition from the inner valence band to the impurity energy levels, as shown in Figure 2f.

As for the FAI-T surface, the peaks of ε_2 for the three cases (clean FAI-T, SnF_2 adsorption, and SnF_4 adsorption on FAI-T) are at 1.67 eV coincidentally, implying that SnF_2 or SnF_4 do not affect the degree of direct transition. Apparently, SnF_2 adsorption decreases the static dielectric constant, while SnF_4 adsorption enhances it. Hence, we judge that SnF_2 adsorption

https://doi.org/10.1021/acsomega.1c00767
ACS Omega 2021, 6, 14938−14951

decreases the surface polarization effect, and SnF_4 adsorption increases the surface polarization effect on perovskite.

All in all, it generates a peak in the SnF_4 adsorption on the SnI_2-T surface case, with the electrons jumping from the impurity level to the conduction band. In addition, SnF_4 adsorption improves the static dielectric function of the FAI-T surface and increases the polarization properties of $FASnI_3$.

4. CONCLUSIONS

In summary, this work explores the impacts of SnF_2 and SnF_4 molecules adsorbed on the FAI-T and SnI_2-T surface of $FASnI_3$ based on the first-principles method. By analyzing the total energy and adsorption energy, we found that the case of S2 has the smallest adsorption energy of 0.5376 eV. In the band structure, SnF_2 molecules broaden the band gap of each surface. Interestingly, each case of SnF_4 molecule adsorption on the two surfaces induced impurity energy levels in their band gaps. By analyzing the band structures and the effective masses, on the one hand, SnF_2 and SnF_4 weaken the carrier effective masses on the SnI_2-T surface, except for the case where SnF_4 increases the hole effective mass of the FAI-T surface. On the other hand, in other cases, for SnF_2 or SnF_4 adsorption on the FAI-T surface, the carrier effective masses are both reduced. Therefore, by the electron effective mass analysis, selecting SnF_2 is much more efficient as it possesses a smaller electron effective mass with higher mobility. These results indicate that SnF_2 strengthened the Sn−I bond and even boosted the $[SnI_6]^{4-}$ octahedral structures.

Lastly, in the aspect of optical properties, including the dielectric function and absorbance spectrum, SnF_2 makes the perovskite possess higher absorption coefficient than SnF_4. Especially, for the dielectric function, SnF_4 molecules affect ε_2 largely. This means that SnF_2 adsorption made it easier for the perovskite to respond to an external electric field than SnF_4 adsorption did. All in all, SnF_2 adsorption effects are superior to those of SnF_4 in the photovoltaic application of $FASnI_3$.

Then, it is proposed that adding SnF_2 into perovskite at an appropriate proportion is effective in enhancing the photoelectric performance of perovskite. Meanwhile, SnF_4 added into perovskite diminishes the optical property of perovskite as a shallow acceptor. Thus, Sn(II) is positive in terms of promoting the photoelectric performance of perovskite, and Sn(IV) is negative. In addition, the role of the F^- ion is significant in enhancing the performance when SnF_2 is added into perovskite as it has an interaction with the FA^+ cation, forming a N−H···F hydrogen bond, promoting the charge transfer of protons in the FA^+ cation. In this regard, adding fluoride into the perovskite can also improve the photoelectric performance of perovskite.

■ ASSOCIATED CONTENT

Supporting Information

The Supporting Information is available free of charge at https://pubs.acs.org/doi/10.1021/acsomega.1c00767.

Surface defect state calculation details, surface defects and their formation energy, defect level, and band gap (PDF)

■ AUTHOR INFORMATION

Corresponding Author

Neng Li − *State Key Laboratory of Silicate Materials for Architectures, Wuhan University of Technology, Wuhan 430070, P.R. China; Shenzhen Research Institute of Wuhan University of Technology, Shenzhen 518000, China; State Center for International Cooperation on Designer Low-Carbon & Environmental Materials (CDLCEM), School of Materials Science and Engineering, Zhengzhou University, Zhengzhou 450001, Henan, China;* orcid.org/0000-0001-9633-6702; Email: lineng@whut.edu.cn

Authors

Wei Xie − *College of Physics and Telecommunications, Huanggang Normal University, Huangzhou 438000, P.R. China*

Liping Peng − *College of Physics and Telecommunications, Huanggang Normal University, Huangzhou 438000, P.R. China*

Complete contact information is available at: https://pubs.acs.org/10.1021/acsomega.1c00767

Notes

The authors declare no competing financial interest.

■ ACKNOWLEDGMENTS

W.X. and L.P. gratefully acknowledge financial support from the Scientific Research Project of Hubei Education Department (grant no. D20182901), Breeding Program Funds for Huanggang Normal University (grant no. 04201813603), and Huanggang Science and Technology Project (grant no. XQYF2018000013). N.L. acknowledges financial support from the Natural Science Fund for Distinguished Young Scholars of Hubei Province (no. 2020CFA087), the Fok Ying-Tong Education Foundation for Young Teachers in the Higher Education Institutions of China (no. 161008), the Basic Research Program of Shenzhen (no. JCYJ20190809120015163), and the Overseas Expertise Introduction Project (111 project) for Discipline Innovation of China (No. B18038).

■ REFERENCES

(1) Kojima, A.; Teshima, K.; Shirai, Y.; Miyasaka, T. Organometal Halide Perovskites as Visible-Light Sensitizers for Photovoltaic Cells. *J. Am. Chem. Soc.* **2009**, *131*, 6050−6051.

(2) Hu, Z.; Zeng, Y.; Li, X.; Meng, L. Enhancing the Stability of Perovskites by Constructing Heterojunctions of Graphene/$MASnI_3$. *Phys. Chem. Chem. Phys.* **2020**, *22*, 3724−3733.

(3) Kim, H.-S.; Lee, C.-R.; Im, J.-H.; Lee, K.-B.; Moehl, T.; Marchioro, A.; Moon, S.-J.; Humphry-Baker, R.; Yum, J.-H.; Moser, J. E.; Grätzel, M.; Park, N.-G. Lead iodide perovskite sensitized all-solid-state submicron thin film mesoscopic solar cell with efficiency exceeding 9%. *Sci. Rep.* **2012**, *2*, 591.

(4) Lee, M. M.; Teuscher, J.; Miyasaka, T.; Murakami, T. N.; Snaith, H. J. Efficient hybrid solar cells based on meso-superstructured organometal halide perovskites. *Science* **2012**, *338*, 643−647.

(5) Liu, M.; Johnston, M. B.; Snaith, H. J. Efficient planar heterojunction perovskite solar cells by vapour deposition. *Nature* **2013**, *501*, 395−398.

(6) Xiao, Z.; Bi, C.; Shao, Y.; Dong, Q.; Wang, Q.; Yuan, Y.; Wang, C.; Gao, Y.; Huang, J. Efficient, high yield perovskite photovoltaic devices grown by interdiffusion of solution-processed precursor stacking layers. *Energy Environ. Sci.* **2014**, *7*, 2619−2623.

(7) Jeon, N. J.; Noh, J. H.; Kim, Y. C.; Yang, W. S.; Ryu, S.; Seok, S. I. Solvent engineering for high-performance inorganic-organic hybrid perovskite solar cells. *Nat. Mater.* **2014**, *13*, 897−903.

(8) Wang, L.; Zhou, H.; Hu, J.; Huang, B.; Sun, M.; Dong, B.; Zheng, G.; Huang, Y.; Chen, Y.; Li, L.; et al. A Eu^{3+}-Eu^{2+} ion redox

shuttle imparts operational durability to Pb-I perovskite solar cells. *Science* **2019**, *363*, 265.
(9) Zhou, H.; Chen, Q.; Li, G.; Luo, S.; Song, T.-B.; Duan, H.-S.; Hong, Z.; You, J.; Liu, Y.; Yang, Y. Interface engineering of highly efficient perovskite solar cells. *Science* **2014**, *345*, 542−546.
(10) Yang, W. S.; Noh, J. H.; Jeon, N. J.; Kim, Y. C.; Ryu, S.; Seo, J.; Seok, S. I. High-performance photovoltaic perovskite layers fabricated through intramolecular exchange. *Science* **2015**, *348*, 1234−1237.
(11) Kaake, L.; Dang, X.-D.; Leong, W. L.; Zhang, Y.; Heeger, A.; Nguyen, T.-Q. Effects of impurities on operational mechanism of organic bulk heterojunction solar cells. *Adv. Mater.* **2013**, *25*, 1706−1712.
(12) Bi, D.; Tress, W.; Dar, M. I.; Gao, P.; Luo, J.; Renevier, C.; Schenk, K.; Abate, A.; Giordano, F.; Correa Baena, J.-P.; et al. Efficient luminescent solar cells based on tailored mixed-cation perovskite. *Sci. Adv.* **2016**, *2*, No. e1501170.
(13) Mei, A.; Li, X.; Liu, L.; Ku, Z.; Liu, T.; Rong, Y.; Xu, M.; Hu, M.; Chen, J.; Yang, Y.; et al. A hole-conductor-free, fully printable mesoscopic perovskite solar cell with high stability. *Science* **2014**, *345*, 295−298.
(14) Chen, W.; Wu, Y.; Yue, Y.; Liu, J.; Zhang, W.; Yang, X.; Chen, H.; Bi, E.; Ashraful, I.; Grätzel, M.; Han, L. Efficient and Stable Large-Area Perovskite Solar Cells with Inorganic Charge Extraction Layers. *Science* **2015**, *350*, 944−948.
(15) Niu, G.; Guo, X.; Wang, L. Review of recent progress in chemical stability of perovskite solar cells. *J. Mater. Chem. A* **2015**, *3*, 8970.
(16) Heo, J. H.; Kim, J.; Kim, H.; Moon, S. H.; Im, S. H.; Hong, K.-H. Roles of SnX_2 (X = F, Cl, Br) Additives in Tin-Based Halide Perovskites toward Highly Efficient and Stable Lead-Free Perovskite Solar Cells. *J. Phys. Chem. Lett.* **2018**, *9*, 6024−6031.
(17) Noel, N. K.; Stranks, S. D.; Abate, A.; Wehrenfennig, C.; Guarnera, S.; Haghighirad, A.-A.; Sadhanala, A.; Eperon, G. E.; Pathak, S. K.; Johnston, M. B.; et al. Lead-free organic-inorganic tin halide perovskites for photovoltaic applications. *Energy Environ. Sci.* **2014**, *7*, 3061−3068.
(18) Liao, W.; Zhao, D.; Yu, Y.; Grice, C.; Wang, C.; Cimaroli, A.; Schulz, P.; Meng, W.; Zhu, K.; Xiong, R.-G.; et al. Lead-Free Inverted Planar Formamidinium Tin Triiodide Perovskite Solar Cells Achieving Power Conversion Efficiencies up to 6.22%. *Adv. Mater.* **2016**, *28*, 9333−9340.
(19) Zhang, T.; Sun, Q.; Zhang, X.; Shen, Y. d.; Wan, M. Minimizing energy lossin two-dimensional tin halide perovskite solarcells-Aperspective. *APL Mater.* **2021**, *9*, 020906.
(20) Liao, Y.; Liu, H.; Zhou, W.; Yang, D.; Shang, Y.; Shi, Z.; Li, B.; Jiang, X.; Zhang, L.; Quan, L. N.; et al. Highly Oriented Low-Dimensional Tin Halide Perovskites with Enhanced Stability and Photovoltaic Performance. *J. Am. Chem. Soc.* **2017**, *139*, 6693−6699.
(21) Ke, W.; Stoumpos, C. C.; Zhu, M.; Mao, L.; Spanopoulos, I.; Liu, J.; Kontsevoi, O. Y.; Chen, M.; Sarma, D.; Zhang, Y.; et al. Enhanced photovoltaic performance and stability with a new type of hollow 3D perovskite {en}$FASnI_3$. *Sci. Adv.* **2017**, *3*, No. e1701293.
(22) Zong, Y.; Zhou, Z.; Chen, M.; Padture, N. P.; Zhou, Y. Lewis-Adduct Mediated Grain-Boundary Functionalization for Efficient Ideal-Bandgap Perovskite Solar Cells with Superior Stability. *Adv. Energy Mater.* **2018**, *8*, 1800997.
(23) Lee, S. J.; Shin, S. S.; Kim, Y. C.; Kim, D.; Ahn, T. K.; Noh, J. H.; Seo, J.; Seok, S. I. Fabrication of Efficient Formamidinium Tin Iodide Perovskite Solar Cells through SnF(2)-Pyrazine Complex. *J. Am. Chem. Soc.* **2016**, *138*, 3974−3977.
(24) Tatiana, S.-M.; Wiria, S.; Monica, M.-M. Pressing challenges of halide perovskite thin film growt. *APL Mater.* **2020**, *8*, 110903.
(25) Tai, Q.; Guo, X.; Tang, G.; You, P.; Ng, T.-W.; Shen, D.; Cao, J.; Liu, C.-K.; Wang, N.; Zhu, Y.; et al. Antioxidant Grain Passivation for Air-Stable Tin-Based Perovskite Solar Cells. *Angew. Chem., Int. Ed.* **2019**, *58*, 806−810.
(26) Zhu, Z.; Chueh, C. C.; Li, N.; Mao, C.; Jen, A. K. Realizing Efficient Lead-Free Formamidinium Tin Triiodide Perovskite Solar Cells via a Sequential Deposition Route. *Adv. Mater.* **2018**, *30*, 1703800.
(27) Gao, Y.; Shi, E.; Deng, S.; Dou, L. Molecular engineering of organic−inorganic hybrid perovskites quantum wells, Molecular engineering of organic−inorganic hybrid perovskites quantum wells. *Nat. Chem.* **2019**, *11*, 1151−1157.
(28) Kresse, G.; Furthmüller, J. Efficiency of ab-initio total energy calculations for metals and semiconductors using a plane-wave basis set. *Comput. Mater. Sci.* **1996**, *6*, 15−50.
(29) Perdew, J. P.; Wang, Y. Accurate and simple analytic representation of the electron-gas correlation energy. *Phys. Rev. B* **1992**, *45*, 13244−13249.
(30) Schueller, E. C.; Laurita, G.; Fabini, D. H.; Stoumpos, C. C.; Kanatzidis, M. G.; Seshadri, R. Crystal Structure Evolution and Notable Thermal Expansion in Hybrid Perovskites Formamidinium Tin Iodide and Formamidinium Lead Bromide. *Inorg. Chem.* **2018**, *57*, 695−701.
(31) Perdew, J. P.; Burke, K.; Ernzerhof, M. Generalized Gradient Approximation Made Simple. *Phys. Rev. Lett.* **1996**, *77*, 3865−3868.
(32) Zhang, Z.; Fang, W. H.; Long, R.; Prezhdo, O. V. Exciton Dissociation and Suppressed Charge Recombination at 2D Perovskite Edges: Key Roles of unsaturated halide bonds and thermal disorder. *J. Am. Chem. Soc.* **2019**, *141*, 15557−15566.
(33) ((a)) Coles, B.R.; Caplin, A.D.; Hall, H.E. *The Electronic Structures of Solids Solid state physics*; 1974. ((b)) Ashhcroft, N. W.; Mermin, N. D. *Solid State Physics*; saunders college, Philadelphia, 1976.
(34) Dang, Y.; Zhou, Y.; Liu, X.; Ju, D.; Xia, S.; Xia, H.; Tao, X. Formation of Hybrid Perovskite Tin Iodide Single Crystals by Top-Seeded Solution Growth. *Angew. Chem. Int. Ed. Engl.* **2016**, *55*, 3447−3450.
(35) Koh, T. M.; Krishnamoorthy, T.; Yantara, N.; Shi, C.; Leong, W. L.; Boix, P. P.; Grimsdale, A. C.; Mhaisalkar, S. G.; Mathews, N. Formamidinium tin-based perovskite with low Eg for photovoltaic applications. *J. Mater. Chem. A* **2015**, *3*, 14996.
(36) Eperon, G. E.; Stranks, S. D.; Menelaou, C.; Johnston, M. B.; Herz, L. M.; Snaith, H. J. Formamidinium lead trihalide: a broadly tunable perovskite for efficient planar heterojunction solar cells. *Energy Environ. Sci.* **2014**, *7*, 982−988.
(37) Pang, S.; Hu, H.; Zhang, J.; Lv, S.; Yu, Y.; Wei, F.; Qin, T.; Xu, H.; Liu, Z.; Cui, G. $NH_2CH{=}NH_2PbI_3$: An Alternative Organolead Iodide Perovskite Sensitizer for Mesoscopic Solar Cells. *Chem. Mater.* **2014**, *26*, 1485−1491.
(38) Nishikubo, R.; Ishida, N.; Katsuki, Y.; Wakamiya, A.; Saeki, A. Minute-Scale Degradation and Shift of Valence-Band Maxima of $(CH_3NH_3)SnI_3$ and $HC(NH_2)_2SnI_3$ Perovskites upon Air Exposure. *J. Phys. Chem. C* **2017**, *121*, 19650−19656.
(39) Ma, X.-X.; Li, Z.-S. The effect of oxygen molecule adsorption on lead iodide perovskite surface by first-principles calculation. *Appl. Surf. Sci.* **2018**, *428*, 140−147.
(40) Geng, W.; Zhang, L.; Zhang, Y.-N.; Lau, W.-M.; Liu, L.-M. First-Principles Study of Lead Iodide Perovskite Tetragonal and Orthorhombic Phases for Photovoltaics. *J. Phys. Chem. C* **2014**, *118*, 19565−19571.
(41) Feng, Z.; Hu, H.; Cui, S.; Bai, C. First-principles study of optical properties of $SrZrO_3$ in cubic phase. *Solid State Commun.* **2008**, *148*, 472−475.
(42) Pauling, L. The energy of single bonds and the relative electronegativity of atoms. *J. Am. Chem. Soc.* **1932**, *54*, 3570−3582.
(43) Mante, P. A.; Stoumpos, C. C.; Kanatzidis, M. G.; Yartsev, A. Electron-acoustic phonon coupling in single crystal $CH_3NH_3PbI_3$ perovskites revealed by coherent acoustic phonons. *Nat. Commun.* **2017**, *8*, 14398.
(44) Wang, Y.; Zhang, Y.; Zhang, P.; Zhang, W. High intrinsic carrier mobility and photon absorption in the perovskite $CH_3NH_3PbI_3$. *Phys. Chem. Chem. Phys.* **2015**, *17*, 11516−11520.
(45) Bardeen, J.; Shockley, W. Deformation potentials and mobilities in non-polar crystals. *Phys. Rev.* **1950**, *80*, 72.

https://doi.org/10.1021/acsomega.1c00767
ACS Omega 2021, 6, 14938−14951

(46) Fuentealba, P.; Chamorro, E.; Santos, J. C. Chapter 5, Understanding and using the electron localization function. Theoretical Aspects of Chemical Reactivity. *Theor. Comput. Chem.* **2007**, 57−85.
(47) Fuster, F.; Sevin, A.; Silvi, B. Topological Analysis of the Electron Localization Function (ELF) Applied to the Electrophilic Aromatic Substitution. *J. Phys. Chem. A.* **2000**, *104*, 852−858.
(48) Noury, S.; Colonna, F.; Savin, A.; Silvi, B. Analysis of the delocalization in the topological theory of chemical bond. *J. Mol. Struct.* **1998**, *450*, 59−68.
(49) Sahni, V.; Pan, X. Y. Quantal density functional theory of degenerate states. *Phys. Rev. Lett.* **2003**, *90*, 123001.
(50) Thanopulos, I.; Král, P.; Shapiro, M. Complete Control of Population Transfer between Clusters of Degenerate States. *Phys. Rev. Lett.* **2004**, *92*, 113003.
(51) Luo, J. J.; Wang, X. M.; Li, S. R.; Liu, J.; Guo, Y. M.; Niu, G. D.; Yao, L.; Fu, Y. H.; Gao, L.; Dong, Q. S.; et al. Efficient and stable emission of warm-white light from lead-free halide double perovskites. *Nature* **2018**, *563*, 541.
(52) Li, S.; Luo, J.; Liu, J.; Tang, J. Self-Trapped Excitons in All-Inorganic Halide Perovskites: Fundamentals, Status, and Potential Applications. *J. Phys. Chem. Lett.* **2019**, *10*, 1999−2007.
(53) Li, N.; Tao, S.; Chen, Y.; Niu, X.; Onwudinanti, C. K.; Hu, C.; Qiu, Z.; Xu, Z.; Zheng, G.; Wang, L.; et al. Cation and anion immobilization through chemical bonding enhancement with fluorides for stable halide perovskite solar cells. *Nat. Energy* **2019**, *4*, 408−415.
(54) Moulder, J.F. *Handbook of X-ray photoelectron spectroscopy*; Perkin-Elmer Corp: Eden, Prairie, 1992.
(55) Scipioni, R.; Gazzoli, D.; Teocoli, F.; Palumbo, O.; Paolone, A.; Ibris, N.; Brutti, S.; Navarra, M. A. Preparation and Characterization of Nanocomposite Polymer Membranes Containing Functionalized SnO_2 Additives. *Membranes* **2014**, *4*, 123.
(56) Noel, N. K.; Abate, A.; Stranks, S. D.; Parrott, E. S.; Burlakov, V. M.; Goriely, A.; Snaith, H. J. Enhanced Photoluminescence and Solar Cell Performance via Lewis Base Passivation of Organic-Inorganic Lead Halide Perovskites. *ACS Nano* **2014**, *8*, 9815.
(57) Tricker, M. J.; Donaldson, J. D. Comments on the Structure, Bonding and 119Sn Mössbauer Parameters of Tin(II) Derivatives of the Type $MSnX_3$. *Inorg. Chem. Acta.* **1978**, *31*, L445.
(58) Hildebrandt, J. Coupled two-quantum-transition probability for laser photons and microwave plasmons. *Opt. Lett.* **1985**, *10*, 541−543.

https://doi.org/10.1021/acsomega.1c00767
ACS Omega 2021, 6, 14938−14951